

Article

Entropy Generation of CuO-Water Nanofluid in a Cavity with an Intruded Rectangular Fin

Periklis Mountrichas, Wendi Zhao, Mehtab Singh Randeva and Prodip K. Das * 

School of Engineering, Newcastle University, Newcastle NE1 7RU, UK

* Correspondence: prodip.das@newcastle.ac.uk; Tel.: +44-191-208-6170

Abstract: Entropy generation and heat transfer in cavities have received significant interest due to the ever-increasing demand for enhancing thermal performances in many scientific and engineering fields. In particular, nanofluids are being used increasingly in engineering applications and real-life problems, as they exhibit significantly better thermal properties than basic heat transfer fluids, for example, water, oil, or ethylene glycol. This study investigates the entropy generation and heat transfer of a nanofluid in a confined cavity with a moving top wall and a rectangular fin at the bottom. Here, a macro-homogeneous model based on a previously developed model is employed for investigating the mixed convective flow and heat transfer of CuO-water nanofluid. Various fin geometries, Rayleigh numbers, Reynolds numbers, and nanofluid concentrations have been employed. Present results indicate that the heat transfer rate can be improved, while entropy generation can be minimized using nanofluids instead of conventional heat transfer fluids.

Keywords: constructal design; entropy generation; fin; heat transfer; mixed convection; nanofluid



Citation: Mountrichas, P.; Zhao, W.; Randeva, M.S.; Das, P.K. Entropy Generation of CuO-Water Nanofluid in a Cavity with an Intruded Rectangular Fin. *Energies* **2023**, *16*, 912. <https://doi.org/10.3390/en16020912>

Academic Editors: Frede Blaabjerg and Paul Stewart

Received: 7 December 2022

Revised: 7 January 2023

Accepted: 11 January 2023

Published: 13 January 2023



Copyright: © 2023 by the authors. Licensee MDPI, Basel, Switzerland. This article is an open access article distributed under the terms and conditions of the Creative Commons Attribution (CC BY) license (<https://creativecommons.org/licenses/by/4.0/>).

1. Introduction

The mixed convection of heat transfer in cavities has been one of the most important topics in the engineering sector of thermofluid dynamics [1–6]. Mixed convection exists when both forced and natural convection have influences, and its analysis is complex due to the buoyancy and shear forces and their complex interactions [5]. Due to the widely used applications of heat transfer in energy storage systems, cooling of electronic devices, nuclear reactors, and heating of rooms or buildings, etc., it is of great importance to ensure its safety and efficiency [6]. Several methods have recently been applied to increase heat transfer performance, for example, altering the boundary conditions [6–10], geometry, and flow domains [11–15], and, most importantly, improving working fluid's thermal properties [16–19]. According to previous research, it has been established that the thermal properties of conventional heat transfer fluids, such as water, oil, or ethylene glycol, can be enhanced by transforming them into nanofluids.

Nanofluids can be created by adding a considerable number of nanoparticles in a conventional heat transfer fluid, with at least one of their principal dimensions lower than 100 nm. Studies have shown that nanofluids have enhanced thermal properties, for example, thermal diffusivity, conductivity, viscosity, and heat transfer coefficients which are all responsible for higher efficiency than that of a base fluid [19–21]. Numerous studies, including, but not limited to, Cong et al. [1], Ting et al. [4], Buongiorno et al. [16], Lee et al. [19], Tiwari et al. [22], Talebi et al. [23], and Mansour et al. [24] have been conducted and, either by using CuO-water or Al₂O₃-water nanofluid, have shown that the heat transfer increases with nanoparticle concentrations. Recently, Atashafrooz [25] investigated the effects of buoyancy force on mixed convection heat transfer and entropy generation. It was concluded that an increase in the amounts of flow irreversibility is possible by enhancing the buoyancy force and nanoparticles concentration. In his latest work on entropy generation for forced convection [26], it was once again concluded that the rates of flow

irreversibility enhance significantly with the nanoparticle concentrations. According to the study of Khanafer et al. [18], heat transfer in the cavity increases as the concentration of the nanoparticles increases. Oztop and Abu-Nada [7] also showed a higher heat transfer rate with higher nanoparticle concentrations. Despite the fact that many studies have been conducted for establishing the more efficient thermal performance of nanofluids, further studies are vital to show that higher nanofluid thermal properties are advantageous for mixed convection heat transfer in cavities [4]. As conductive nanoparticles in conventional heat transfer fluid also increase the fluid's density, the nanofluid's overall thermal performance can be dependent on nanoparticle and base fluid's properties, a trade-off between various thermophysical properties of nanofluid can be vital. Moreover, thermal conductivity itself may not be a limiting criterion for improving thermal performances with nanofluids, particularly in a situation where both natural convection and mixed convection are dominant. As indicated in Ref. [27], nanoparticles with high thermal conductivity are not always a suitable option to enhance the thermal performance of a nanofluid compared with a conventional heat transfer fluid. There can also be controversy on whether a nanofluid enhances the overall thermal performance for applications, where mixed convection performs the dominant role. Therefore, it is important to explore the mixed convection of nanofluids and the thermal and geometric optimization with nanofluids.

When a fluid is driven due to buoyancy force caused by the temperature difference is considered natural convection. Conversely, in forced convection, the fluid is driven by an external force, e.g., a moving wall which drives the fluid resulting in a forced flow [8]. Mixed convection is a mixture under both natural and forced convection conditions [4], and it is the most preferred mode to enhance heat transfer. However, mixed convection in a cavity can be complex to analyse, and it will be appreciated that a full study of heat transfer in laminar flow in a cavity, including entrance length effects, different thermal boundary conditions, variable properties, etc., requires years of research. This mode of convection is used widely with lots of applications, especially in the industry. Applications, such as production machinery, internal combustion engines, petroleum refineries, power generation, technologies requiring lubrication, and food or other products processing, are driven by advanced nanofluids due to their high thermal capabilities [1].

Another key parameter for validating the quality and performance of a nanofluid is entropy generation. The second law of thermodynamics is the mechanism to be used in cavity problems to calculate the entropy generations caused by heat transfer and fluid friction in the cavity and hence minimize it [6]. It is always of great matter to minimize the entropy generation because it reduces the thermodynamic efficiency and hence the performance of the system. Thus, the geometry has to be modified so that the useful work (energy) is not destroyed by convection [28]. There is a large number of experimental and numerical articles available in the open literature for the optimization of fins and cavities using the constructal design method. Most of these studies are for cavities with conventional heat transfer fluids [29–34]. The constructal design method has not been rigorously utilized for nanofluids. In addition, the investigation of nanofluid's mixed convective flow and heat transfer in cavities with intruded fins and their optimization using the constructal design method is still elusive [1,35].

In a lid-driven cavity filled with nanofluid, the issue of entropy generation has been a major concern for many researchers. Numerous studies have been done to investigate the causes and find solutions. According to Cho [36], as the concentration of Al_2O_3 nanoparticles increases, the total entropy generation decreases, and the Nusselt number increases. However, Atashafrooz and his team [25,26] concluded that flow irreversibility increases with the nanoparticle concentrations. There is also the option of changing the geometry of the cavity which may affect the entropy generation. The research of Oliveski et al. [37] highlighted that the entropy generation under steady-state natural convection conditions increases linearly with the aspect ratio and exponentially with the Rayleigh number. Furthermore, their study indicated that for the same aspect ratio, entropy generation increases with the Rayleigh number (Ra) because of viscous effects. According to Ilis et al. [6], many

models and geometries for heat transfer in a cavity have been created to determine the main cause of entropy generation; however, it seems that is formed mostly due to heat transfer for $Ra < 10^5$, whereas for $Ra > 10^5$ fluid friction has the biggest contribution.

Even though there is a great number of investigations already done on entropy generation and its causes, there are still several thermodynamic uncertainties. Particularly, the advantages of using nanofluids, any geometry or surface feature, and the impact of nanofluids, such as CuO-water nanofluid, on entropy generation and heat transfer have to be researched more to discover new aspects. Therefore, this study examines the effects of CuO-water nanofluid on entropy generation and heat transfer into the light by changing nanoparticle concentrations and the geometry of the cavity. A square cavity with an intruded rectangular fin and a moving wall at a constant velocity filled with CuO-water nanofluid has been considered in the present investigation. This investigation includes simulations of different Rayleigh and Reynolds numbers, several nanoparticle concentrations, and different fin aspect ratios. The entropy generations as a result of heat transfer irreversibility and fluid friction have also been evaluated along with the Bejan and Nusselt numbers. In continuation of our previous study [1], we examine the entropy generation and heat transfer of CuO-water nanofluid using the previously developed macro-homogeneous model and analyse various flow parameters for which the heat transfer of CuO-water nanofluid can be enhanced while minimizing entropy generation. In addition, the constructal design method has been utilized to obtain fin geometry with higher heat transfer and lower entropy generation, where the fin's area and aspect ratio are considered as the degrees of freedom. The details of the constructal design method are available elsewhere [1,29–31].

2. Mathematical Modelling

2.1. Considered Problem

The considered problem is a CuO-water nanofluid flow in a cavity with a rectangular fin intruded from the bottom surface, which is adapted from Ref. [1], and the schematic diagram of the domain is shown in Figure 1. This geometry can potentially be applied to many engineering applications, where an extended surface or fin is used for enhancing heat transfer. For example, it can be used for electronic cooling for faster heat removal, increasing heat transfer performance in solar collectors, and cooling of nuclear rods in a nuclear power plant by improving the functionality of the existing system. The present geometry includes symmetrical conditions at the left and right surfaces. The top wall moves along the x -direction, while it maintains a constant temperature (T_{\min}). The rest of the surfaces are stationary, thus $u^* = 0$ and $v^* = 0$ (dimensionless velocities in x - and y -direction, respectively). The fin area has been defined with a constant but higher temperature of T_{\max} , with an area of A_f , length of L_1 , and height of H_1 . The whole geometry has a length of L , a height of H , and an area of A . All surfaces, except the top one, are defined as adiabatic, and the no-slip condition is applied. The chosen nanofluid is considered Newtonian and incompressible, and the radiation effect has been neglected.

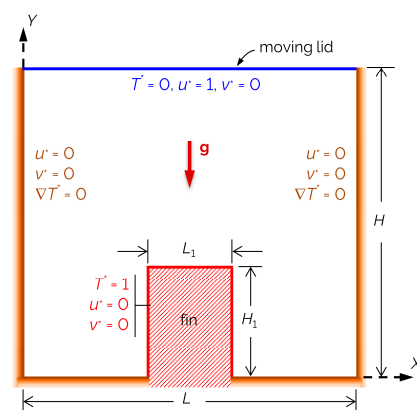


Figure 1. Computational domain with boundary conditions for the investigation of entropy generation CuO-water nanofluid.

The area of the cavity is kept constant while the area of the fin is 5% of the cavity. Uniform size and shape are assumed for the nanoparticles, while their chemical reaction with the water has been neglected. The fin's aspect ratio, AR ($= H_1/L_1$), for the problem is changed from 0.1 to 10. The dimensionless velocity components (u^* and v^*) and temperature (T^*) indicated in Figure 1 are defined according to Ref. [1].

2.2. Governing Mathematical Equations

For the present laminar, two-dimensional, steady-state, mixed convective fluid flow, the governing equations are the conservation equations of mass, momentum, and energy using the Navier–Stokes equation with the Boussinesq approximation in the y -direction for CuO-water nanofluid. These equations can be expressed as [1,4]:

$$\frac{\partial u}{\partial x} + \frac{\partial v}{\partial y} = 0 \quad (1)$$

$$u \frac{\partial u}{\partial x} + v \frac{\partial u}{\partial y} = -\frac{1}{\rho_{nf}} \frac{\partial p}{\partial x} + \frac{\mu_{nf}}{\rho_{nf}} \left(\frac{\partial^2 u}{\partial x^2} + \frac{\partial^2 u}{\partial y^2} \right) \quad (2)$$

$$u \frac{\partial v}{\partial x} + v \frac{\partial v}{\partial y} = -\frac{1}{\rho_{nf}} \frac{\partial p}{\partial y} + \frac{\mu_{nf}}{\rho_{nf}} \left(\frac{\partial^2 v}{\partial x^2} + \frac{\partial^2 v}{\partial y^2} \right) + g\beta_{nf}(T - T_\infty) \quad (3)$$

$$u \frac{\partial T}{\partial x} + v \frac{\partial T}{\partial y} = \frac{k_{nf}}{\rho_{nf}C_{p,nf}} \left(\frac{\partial^2 T}{\partial x^2} + \frac{\partial^2 T}{\partial y^2} \right) \quad (4)$$

where u and v are the flow velocities, p is the static pressure, g is the gravitational acceleration, and the Boussinesq approximation is considered in the y -direction. It is worth noting that the heat due to the nanoparticle's friction with fluid is negligible compared to heat conduction from the heated surface [1]. Thus, the viscous dissipation of energy is neglected in the energy equation. In addition, the Brownian motion of nanoparticles, and the nanoparticle size effects are neglected for simplification by considering low operating temperature and low nanoparticle concentration [4]. For this study, it is assumed at about 10–100 nm diameter, while their shape is considered uniform. However, the size of the nanoparticles can influence heat transfer and fluid flow at high particle concentrations. Thus, careful attention should be given to studies with higher particle concentrations. The effective dynamic viscosity, effective density, effective thermal expansion coefficient, effective thermal conductivity, and effective heat capacity of the macro-homogeneous mixture of CuO nanoparticles and water are defined by μ_{nf} , ρ_{nf} , β_{nf} , k_{nf} , and $C_{p,nf}$, respectively. The density, specific heat capacity, and thermal expansion coefficient of the nanofluid have been obtained by using the effective medium theory, as it has been widely used for multi-phase thermodynamic applications [22,23,38]. The mathematical equations for nanofluid's density, dynamic viscosity, conductivity, specific heat capacity, and thermal expansion coefficient are available in our earlier works [1,4], while CuO nanoparticle and water properties are available in Ref. [39]. During the flow process, inertial and buoyancy forces take place between the particles of the fluid. These forces can be described by dimensionless numbers, such as Reynolds number (Re), Rayleigh number (Ra), and Grashof number (Gr), which are defined as:

$$\text{Re} = \frac{\rho_{nf}u_0H}{\mu_{nf}}; \text{Ra} = \frac{g\beta_{nf}\Delta TH^3}{\nu_{nf}\alpha_{nf}}; \text{Gr} = \frac{g\beta_{nf}\Delta TH^3}{\nu_{nf}} \quad (5)$$

where α_{nf} and ν_{nf} are the nanofluid's thermal diffusivity and kinematic viscosity, respectively. For the different inertial forces, the study has considered Reynolds numbers varied between 10 and 2000, while for the different buoyancy forces, the study has considered Rayleigh numbers varied between 10^3 and 10^7 . The ratio of the buoyancy to the viscous force acting on the fluid is shown by the Grashof number, while the Richardson number can detect the transition point between the natural and forced convection. It has been also found that natural convection dominates when $\text{Ri} > 10$, whereas forced convection

dominates when $Ri < 0.1$. For $0.1 < Ri < 10$, it has been found that both natural and forced convection have an equivalent effect on the flow [40].

To define the heat transfer performance, the use of local and average Nusselt numbers is required. Nusselt number is an important parameter that contributes to a more efficient rate of heat transfer. It represents the enhancement of heat transfer through a fluid layer due to convection across the same fluid layer. The expressions for the local Nusselt number (Nu_l) and the average Nusselt number (Nu_{avg}) are given below:

$$Nu_l = \frac{h_{nf}L}{k_{nf}} \text{ and } Nu_{avg} = \frac{1}{A} \int Nu_l dA \quad (6)$$

The dimensionless entropy generation caused by heat transfer irreversibility (S_{hti}) and fluid friction (S_{ff}) for the present two-dimensional heat and fluid flow in the convection process can be written as [15,28,41]:

$$S_{hti} = \left[\left(\frac{\partial T^*}{\partial X} \right)^2 + \left(\frac{\partial T^*}{\partial Y} \right)^2 \right] \quad (7)$$

$$S_{ff} = \varphi \left[2 \left\{ \left(\frac{\partial u^*}{\partial X} \right)^2 + \left(\frac{\partial v^*}{\partial Y} \right)^2 \right\} + \left(\frac{\partial u^*}{\partial Y} + \frac{\partial v^*}{\partial X} \right)^2 \right] \quad (8)$$

The dimensionless local entropy generation (S_l) is, therefore, the addition of S_{hti} and S_{ff} :

$$S_l = S_{hti} + S_{ff} \quad (9)$$

where φ is the irreversibility distribution ratio and for this study, it has been taken as 10^{-4} . A similar value is considered by Nayak et al. [10], but φ is adjustable depending on the properties of the nanofluid and the boundary conditions of the problem. It can be calculated based on the following equation:

$$\varphi = \frac{S_{ff}}{S_{hti}} = \frac{\mu_{nf}T_0}{k_{nf}} \left(\frac{u_0}{L\Delta T} \right)^2 \quad (10)$$

where u_0 is the velocity of the top moving wall with direction from left to right and magnitude based on the concentration of CuO nanoparticles. The total entropy generation S_t is obtained by integrating the dimensionless local entropy generation S_l over the whole domain. An alternative irreversibility distribution parameter is the Bejan number (Be), which detects whether the heat transfer irreversibility dominates over the fluid friction irreversibility or the opposite. It is also known as the irreversibility distribution, and it is the ratio of entropy generation due to heat transfer to the total entropy generation:

$$Be = \frac{S_{hti}}{S_l} \quad (11)$$

The average Bejan number (Be_{avg}) is obtained by integrating the local Bejan number over the whole domain:

$$Be_{avg} = \frac{1}{V} \int Be dV \quad (12)$$

It is worth noting that for any location in the cavity if $Be \gg 0.5$, the irreversibility due to heat transfer dominates, while if $Be \ll 0.5$, the irreversibility due to fluid friction dominates. When $Be = 0.5$, the irreversibilities due to fluid friction and heat transfer are equal.

3. Numerical Modelling

The set of governing equations is numerically solved by using the finite volume-based software, ANSYS-Fluent considering the associated boundary conditions. A second-order

upwind scheme is used for the spatial discretization of the aforementioned equations. The velocity-pressure coupling is done by the SIMPLE algorithm and the pressure-based solver is used to compute the solution. The solution of the governing equation is considered converged when the residuals are lower than 10^{-6} for the mass and momentum equations and lower than 10^{-8} for the energy equation. Once the converged solution is obtained, the average Nusselt number (Nu_{avg}) is calculated through the integration of the local Nusselt number (Nu_l) over the fin surface using Equation (6). The way Nu_{avg} is defined gives an area-weighted average value which divides the product of selected field variable and cell area by the surface area to give a dimensionless value. The values of Be number and entropy generations caused by heat transfer irreversibility and fluid friction and the total entropy generation have been computed.

3.1. Model Validation

To validate our numerical model and results, various cases are considered. In the first case, a simplified geometry approach is considered based on Nalassamy and Prasad [42] to compare local velocity and temperature. The geometry is like the present case except for the intruded fin and the cavity is filled with pure fluid. It allowed us to reproduce the results of both Nalassamy and Prasad [42], similar to our past work [1]. The full details of this validation case are available in Ref. [1]. We have also compared the Nusselt number calculation with the data of Dixit and Babu [43]. The simulation for this case is performed for the natural convection of air of $Pr = 0.70$ in a square cavity, exactly as in the model of Dixit and Babu [43]. The cavity is made so that the horizontal walls are adiabatic, and the vertical walls are heated with the left wall kept at a higher temperature. The fluid flow is laminar, and the simulation is performed using the Boussinesq approximation, as explained in Section 2.2. Figure 2 shows the average Nusselt number as a function of the Rayleigh number gathered from Dixit and Babu [43] and reproduced in this work. The comparison shown in Figure 2 highlights that an excellent agreement is achieved with the literature data.

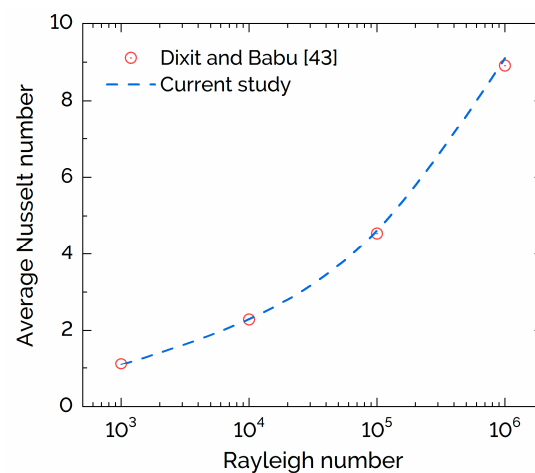


Figure 2. Estimated average Nusselt number of the present study with the benchmark solution of Dixit and Babu [43].

To validate our entropy generation results, another simplified geometry is considered based on Ilis et al. [6], as there are no entropy generation results available in the open literature for the considered problem. The simulation is conducted in a simple natural convection flow in a square cavity filled with air, exactly like the model of Ilis et al. [6]. According to the literature, the cavity considered with insulated (adiabatic) horizontal walls and the vertical walls are maintained at a different temperature, the left wall is kept at T_h and the right wall at T_c satisfying that $T_h > T_c$. A qualitative comparison of the obtained results with the literature results is shown in Figure 3. It can be identified that the

present results about the entropy generations caused by heat transfer irreversibility and fluid friction are in excellent agreement with the results of Ilis et al. [6].

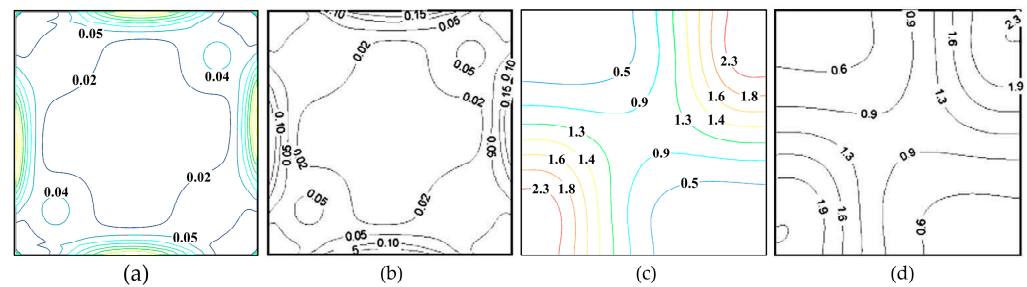


Figure 3. Comparison of local entropy generation contours caused by heat transfer irreversibility (a,b) and caused by fluid friction (c,d). Parts (a,c) show the obtained data, while parts (b,d) show the literature data [6]. Parts (b,d) are reprinted with permission from Ref. [6]. 2008, Elsevier Ltd.

3.2. Mesh Independence Test

It is essential to ensure that the obtained results of numerical analyses are precise, and the choice of the mesh size is prudent and based on test results. This mesh independence test aims to investigate the most appropriate mesh grid size that gives the highest Nusselt number in a relatively short time. It is worth noting the larger the Nusselt number is only the more effective convection. In Figure 4, it is clear that for high mesh sizes, the percentage error (%) remained within 1% or less, which is considered adequately accurate for this study. No numerical issues are noticed during the test procedure considering only that the higher the mesh the longer it took the simulation to run. In addition, all the cases are converged based on the convergence criteria.

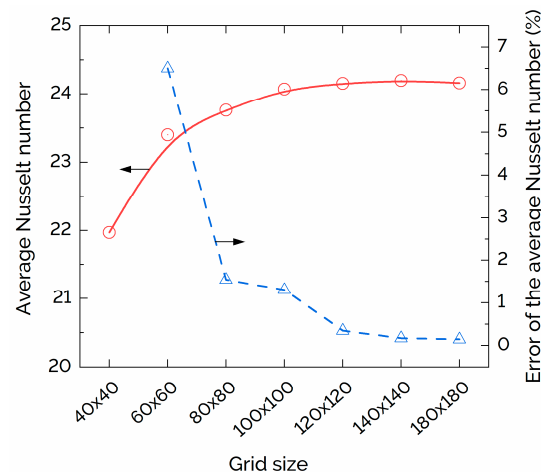


Figure 4. The convergence of Nu_{avg} and its percentage of error for different mesh sizes.

The summarized results of the mesh independence test for all seven different cases are shown in Figure 4. Here, the mesh independence test is done for the base case scenario of this study, which consists of $Ra = 10^5$, $Re = 10^3$, and $\phi = 1\%$ of CuO-water nanofluid in a square cavity, and its geometry of it has an aspect ratio of 0.5. The mesh sizes that are evaluated have a grid size of 40×40 , 60×60 , 80×80 , 100×100 , 120×120 , 140×140 , and 180×180 , respectively. From Figure 4, it can be observed that higher than 100×100 mesh size, the differences in local Nusselt numbers are very small. At first sight, it seems that any mesh of the higher ones would be efficient; however, the 140×140 mesh size provides the highest Nusselt number.

The 180×180 gives a bit lower Nusselt number value than the previous one, probably due to an error of the system, as it is expected to be a bit higher than 140×140 , while it

takes a longer time for the simulation to run. Therefore, the ideal choice stands between mesh grid sizes of 120×120 and 140×140 ; where 140×140 is chosen as it produces the most accurate results, and the percentage of error is less than 0.2%. Although the chosen mesh size requires a higher computational time, the results must be accurate. In addition, Figure 4 shows the percentage (%) in the error of the Nusselt number for all the cases, which is quite low for mesh sizes higher than 100×100 .

4. Numerical Results and Discussion

This section provides numerical results obtained for the mixed convection flow and heat transfer of CuO-water nanofluid in a lid-driven square cavity with an intruded rectangular fin. The numerical results bring into light the optimum fin geometry for maximizing heat transfer and minimizing total entropy generation by varying the strengths of the buoyancy force ($10^3 \leq Ra \leq 10^7$) and the inertial force ($10 \leq Re \leq 2000$) for several values of fin's aspect ratio (AR) keeping cavity size and fin area fraction fixed. The AR of the fin is varied from 0.1 to 10 and the simulations are done for various concentrations of CuO nanoparticles (1% to 5%). A base case parameters scenario has been considered and it consists of $Re = 10^3$, $Ra = 10^5$, 1% CuO nanoparticles, and a fin area fraction of 0.05, and the SIMPLE algorithm is chosen under pressure-based conditions.

4.1. Effects of Fin Aspect Ratio

The local Nusselt numbers (Nu_l) for various fin aspect ratios ($AR = H_1/L_1$) and Re values are presented to demonstrate the effect of the fin aspect ratio on local heat transfer (as shown in Figure 5). Here, Figure 5a shows Nu_l for $Re = 1000$ and Figure 5b shows Nu_l for $AR = 0.1$ along the scaled fin curve length for the base case parameters. It is noticed in Figure 5a that the left side of the fin surface provides higher Nu_l and the right side provides lower Nu_l due to the directions of forced and natural convection. Both forced convection and free convection are acting in the same direction on the fin's left side and in the opposite direction on the fin's right side. The spikes in each line are at the two top corners of the fin, except for $AR = 0.1$, where the highest peak indicates the fin's top surface, and the two smaller peaks at the two ends of the curve are for the fin's top two edges. The maximum value of the local Nusselt number ($Nu_{l,max}$) increases with the fin's AR as it changes from 0.1 to 0.5. However, $Nu_{l,max}$ is lower for $AR = 10$ and higher for $AR = 0.5$. Additionally, Nu_l at the fin's right side is lower for $AR = 10$ compared with the other ARs. Here, the directions of the forced and free convections are opposite on the right side and the cavity is almost divided into two smaller cavities by the fin, where the applied inertial force is acting on the right half of the cavity. Thus, the downward motion of the nanofluid is stronger on the fin's right side for $AR = 10$, which prevents warmer fluid to rise. Additionally, at the lowest AR, only a small portion of nanofluid over the fin's top surface is disturbed by the inertial force; conversely, at the highest AR, the fin penetrates the cavity and separates the convection in two parts making it less efficient and reducing the heat transfer.

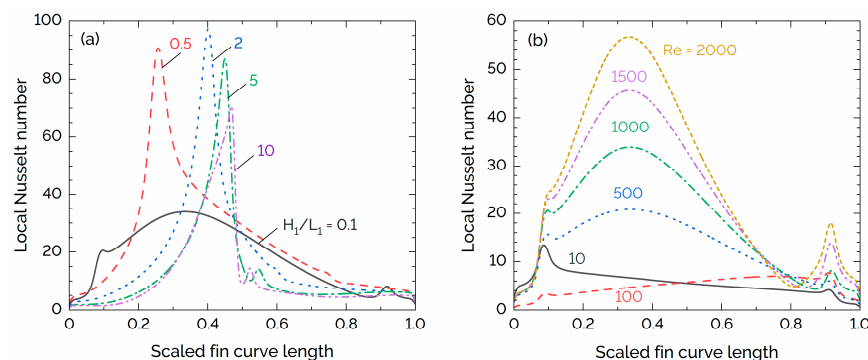


Figure 5. (a) Local Nusselt number with several fin aspect ratios ($AR = H_1/L_1$) for $Re = 1000$ and (b) local Nusselt number with several Reynolds numbers for $AR = 0.1$.

The effects of Reynolds numbers on Nu_f are depicted for the fin aspect ratio of 0.1 in Figure 5b. At low Reynolds numbers ($Re \leq 100$), the inertial force has limited influence on the fluid's movement inside the cavity. Thus, the heat transfer is predominantly diffusive. It is noticed that the local heat transfer is higher from the fin's left surface compared to the top and right surfaces. The local heat transfer is significantly lower at the right surface due to the downward fluid motion as the lid moves in the positive x -direction and the nanofluid circulates clockwise. With the Reynolds numbers, the heat transfer regime starts to shift from the free convection toward the mixed convection regime [1]. Thus, the diffusion on the left-side surface is suppressed by the nanofluid advection, which indicates a higher local heat transfer from the top surface of the fin. A further increase in Reynolds number pushes the mixed convection to the forced convection regime, which allows a higher amount of heat to conduct through the fin and then be transported to the nanofluid from the fin's top surface. This also highlights better displacement of warmer fluid by the colder fluid from the fin surface due to fluid circulation generated by the inertia forces. For the cases of low Reynolds numbers ($Re > 500$), a similar pattern is observed. However, a higher Reynolds number provides a higher peak of Nu_f . Clearly, the higher Reynolds number increases the advection inside the cavity and provides a better heat transfer from the fin surface to the surrounding nanofluid.

4.2. Effects of Inertial and Buoyancy Forces

The effects of inertial and buoyancy forces are analysed by varying the Reynolds numbers between 10 and 2000, and the Rayleigh numbers between 10^3 and 10^7 . Figure 6 shows the scaled Nusselt number (Nu_{avg}/Nu_{max}) as a function of the fin's aspect ratio for $Re = 10$ and 1000, and the average Nusselt number as a function of the Richardson number for various Reynolds numbers as indicated in the figure legend. It has been noticed that heat transfer from the fin surface increases with the fin aspect ratio, then decreases after reaching the maximum Nusselt number. However, the rate of decreasing Nusselt number is larger for $Re = 2000$. As the fin's aspect ratio increases, the flow inside the cavity hinders by the fin and divided into two flow regions on either side of the fin, while at low AR, the flow encounters limited or no obstruction. As the inertial force has limited influence at low Reynolds numbers, the scaled Nusselt number remains higher at higher AR for $Re = 10$, as shown in Figure 6a. Although the Reynolds number increases Nu_{avg} , we noticed that the effects of the Rayleigh number on Nu_{avg} are negligible for the entire range of Reynolds number (10 to 2000) when $Ra \leq 10^5$. Even at a high Rayleigh number ($Ra = 10^6$), the change in Nu_{avg} is small at a high Reynolds number ($Re > 1000$). This can be explained by looking at Figure 6b which shows Nu_{avg} for a function of the Richardson number (Ri) for various values of Reynolds numbers. Figure 6b also highlights the transition of the forced convection to the mixed convection. Changing the Ra number does not change the heat transfer regime as the Richardson number is always less than 0.1 for all Reynolds numbers when $Ra \leq 10^5$. In this case, the dominant heat transfer phenomenon for thermal energy transport is the forced convection remains. Hence, increasing the Reynolds number does not perform any role in the thermal energy transport from the fin to the nanofluid. For higher Rayleigh numbers, the Richardson number changes from 0.034 to 15.5 when the Reynolds number changes from 2000 to 100, and Nu_{avg} increases significantly compared with the other cases, which indicates a higher thermal energy transport from the fin surface. For $Re = 100$ and $Ra = 10^6$, both the forced and free convections perform a combined role in the heat transfer from the fin side surfaces.

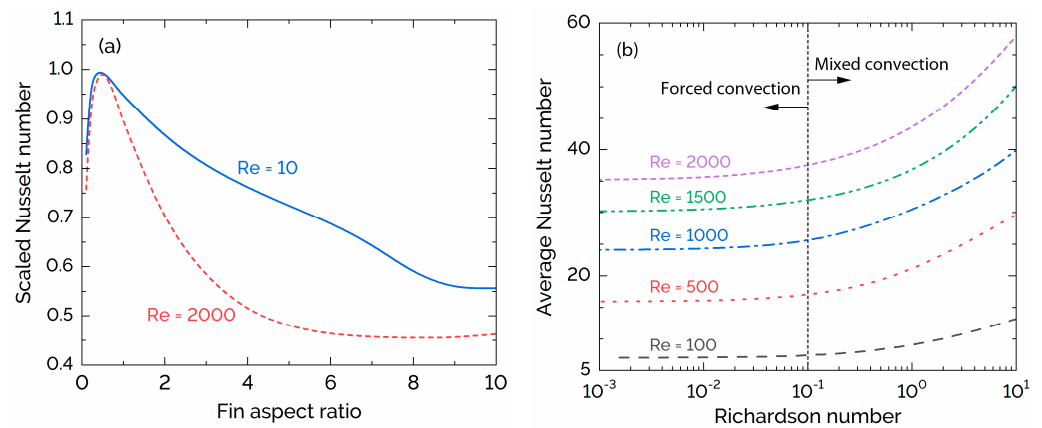


Figure 6. Effects of inertial and buoyancy forces. (a) Scaled Nusselt number as a function of fin aspect ratio for $Re = 10$ and 1000 , and (b) average Nusselt number as a function of the Richardson number for several Reynolds numbers.

4.3. Effects of CuO-Nanoparticle Concentration

To understand the effects of the CuO-nanoparticle concentration in water, Nu_{avg} has been plotted as a function of Reynolds and Rayleigh numbers for four values of particle concentrations. The results are shown in Figure 7, where we observed minor changes in Nu_{avg} with particle concentrations. However, a slight decrease in Nu_{avg} with particle concentration at high Re is noticeable. It is worth mentioning that a 4% CuO-nanoparticle concentration in water effectively increases by about 11% in thermal conductivity than that of water. Hence, we can expect around 11% higher heat conduction from the fin surface to the nanofluid. The higher thermal conductivity of nanofluid reduces Nu_{avg} for a high Reynolds number, as observed in Figure 7a. A similar trend is noticed for various Rayleigh numbers with nanoparticle concentrations, as depicted in Figure 7b. However, the decrease in Nu_{avg} is significant at a low Ra number, particularly in the forced convection regime. These trends further confirm that the relative strength of convective to conduction heat transfer decreases with nanoparticle concentration. Moreover, Nu_{avg} values shown in Figure 7 do not confirm how the convective heat transfer changes with particle concentration in CuO-water nanofluid.

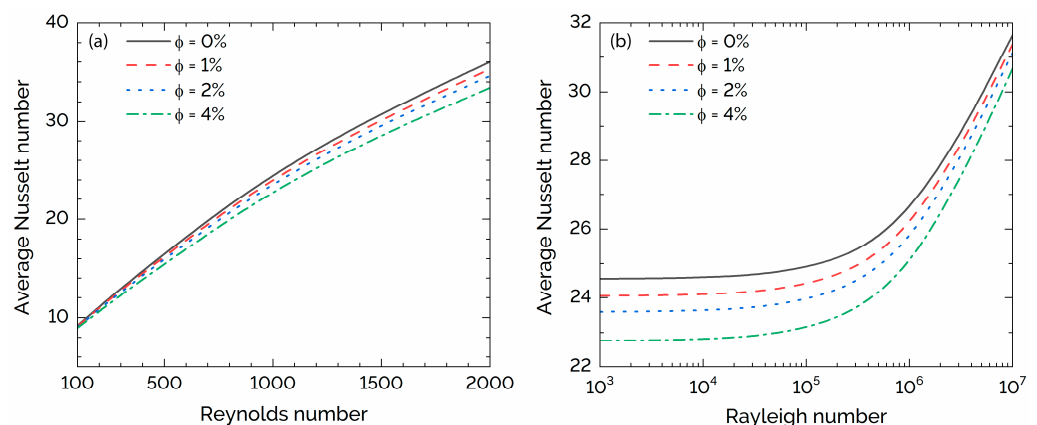


Figure 7. Effects of the concentration of CuO-nanoparticles on Nu_{avg} for four values of particle concentrations. (a) Reynolds number and (b) Rayleigh number.

The convective heat transfer coefficient (h_{nf}) has been further analyzed for four values of nanoparticle concentrations. The results are shown in Figure 8. These results confirm that the convective heat transfer coefficient enhances, as the concentration of CuO-nanoparticle increases. To be specific, at a higher Reynolds number about 4.5% higher h_{nf} can be achieved with a 4% CuO-nanoparticle concentration, while the thermal conductivity of nanofluid

increases by about 11% for the 4% particle concentration. However, the percentage of change in the low Re number is higher, which is about 8% at $Re = 100$. This indicates that nanofluids bring a higher benefit in the mixed convective scenario than in the forced convection case. This is better visualized in Figure 8b, as we see that the changes in h_{nf} are higher at higher Ra numbers. These results provide further insight into how CuO-water nanofluid can be utilized for enhancing heat transfer for engineering applications where mixed convection performs a critical role.

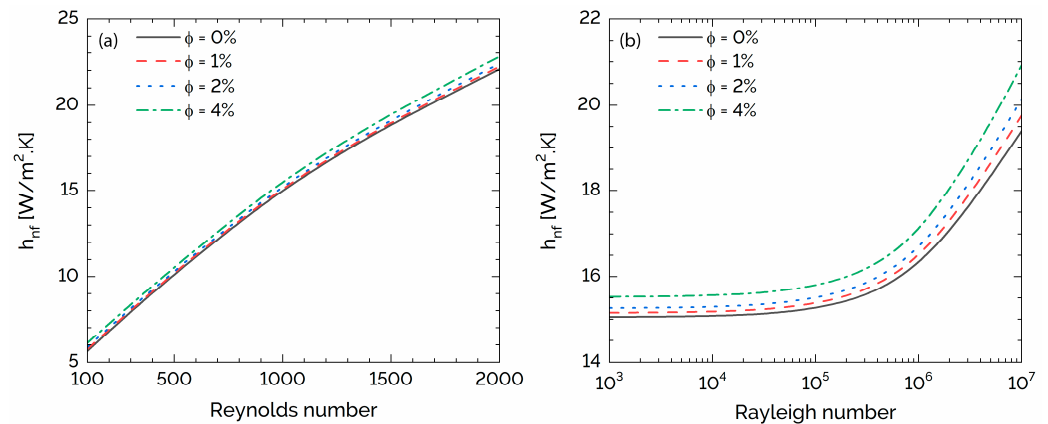


Figure 8. Convective heat transfer coefficient (h_{nf}) with Reynolds and Rayleigh numbers for four values of CuO-nanoparticle concentrations. (a) Reynolds number and (b) Rayleigh number.

4.4. Entropy Generation

This study has also been conducted for the investigation of entropy generations caused by heat transfer irreversibility and fluid friction. Figures 9 and 10 depict the effects of the fin aspect ratio on entropy generation for CuO-water nanofluid. Figure 9 shows the effects of the fin's AR and nanoparticle concentration on entropy generations caused by heat transfer irreversibility and fluid friction. The results shown here are for the base case parameters unless stated in the figure.

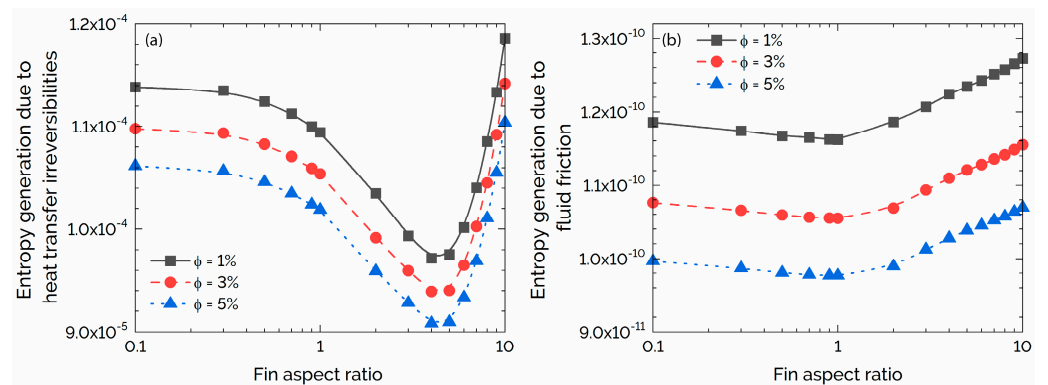


Figure 9. Effects of fin aspect ratio and nanoparticle concentration (ϕ) on entropy generation for CuO-water nanofluid: (a) entropy generation caused by heat transfer irreversibilities and (b) entropy generation caused by fluid friction. The variations are illustrated for $\phi = 1\%$, 3% , and 5% , respectively, and fin area fraction of 0.05, as Re and Ra numbers are kept at 10³ and 10⁵, respectively.

Based on Figure 9a, entropy generation caused by heat transfer irreversibility is high at low aspect ratios, then decreases as the aspect ratio increases until about $AR = 4$ when after that point it starts to dominate again. The lowest entropy generation caused by heat transfer irreversibility value exists for $AR \cong 4$. The contribution of the different concentrations of CuO also has a significant impact. The line of 1% CuO concentration has shown the higher values of entropy generation, while as the concentration increases, the entropy generation

caused by heat transfer irreversibility decreases. The present simulations are performed for several Rayleigh numbers, however, the results showed that there is not any difference to be noted, apart from a not easily detected point at which the natural convection of the flow becomes forced. That transition point is spotted in all three cases at the aspect ratio of about 0.5 and for $Ra \cong 5 \times 10^6$, although the results for this task are not so satisfying to plot. On the other hand, Figure 9b depicts the effects of the different fin aspect ratios on entropy generation caused by fluid friction. Figure 9b depicts that entropy generation caused by fluid friction is low for the lower aspect ratios, as the entropy generation caused by heat transfer irreversibility is dominant for these aspect ratios. However, it is clear that after $AR \cong 1$, the entropy is generated more owing to fluid friction. After that point and up until the highest AR, the trend is kept high without showing signs of getting lower. The effects of the various concentrations are also noticeable. As someone would expect after seeing Figure 9, the fluid friction decreases when the concentration increases. The scientific explanation of this is that all the thermal properties, for example, thermal conductivity, thermal expansion coefficient, and viscosity of the fluid are enhanced; hence, this makes it less frictional between the particles. When comparing these two graphs, one can observe that when AR is around 2, the entropy generations caused by heat transfer irreversibility and fluid friction are balanced, whereas in other cases, only one of them can be considered dominant depending on the geometry of the fin.

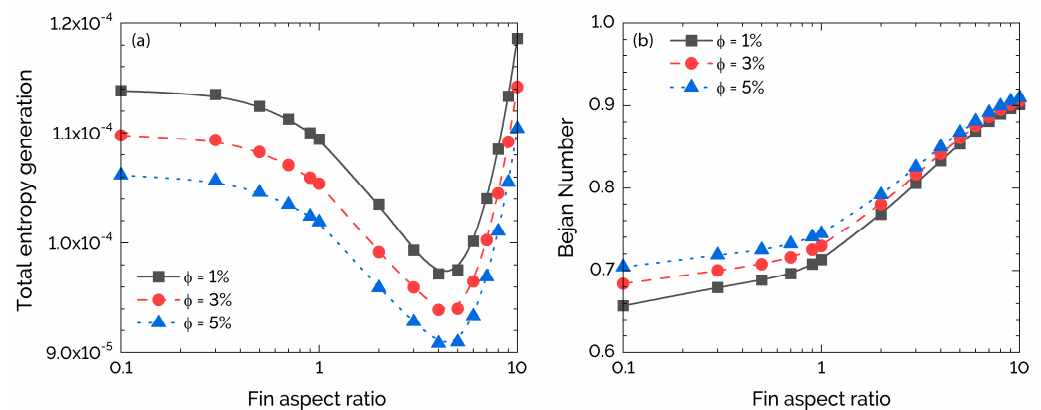


Figure 10. Effects of fin aspect ratio and nanoparticle concentration (ϕ) on entropy generation for CuO-water nanofluid: (a) total entropy generation and (b) average Bejan number.

It is worthwhile to have a look at Figure 10, which includes total entropy generation and Bejan number plots concerning the fin's aspect ratios. The total entropy is generated mainly caused by heat transfer irreversibility, as it is several orders higher than the other. Moreover, the trend shows that it is kept higher at the lowest and the highest aspect ratios, while it decreases as the AR approaches the value of 4. Furthermore, the Bejan number is investigated in detail in Figure 10b. The results are obtained after the integration of local Bejan numbers based on the same parametric values of Ra and Re as previously stated. As the aspect ratio of the fin increases, the Bejan number (Be) increases as well. The rise of Be number is starting linearly. The Be number is the ratio of entropy generation caused by heat transfer irreversibility to the total entropy generation, which means that the higher the fraction is, the less influence the fluid friction forces have. Figure 10b also indicates that since $Be \gg 0.5$ for all the fin aspect ratios and concentrations, the irreversibility caused by heat transfer is dominant in the nanofluid flow. In addition, the higher concentration of CuO results in higher Be number values. Finally, Figure 11 consists of three contours of Be numbers, which depicts an excellent justification supporting the previous graphs, and Figure 10 regarding the trend of Be numbers. Here, the produced contours for aspect ratios of 0.5, 4, and 10 allow us to notice that as the aspect ratio increases, the Be number tends to become 1. This verifies once again what is already stated, with the increase in AR, the entropy generation caused by fluid friction decreases significantly and the

entropy generation caused by heat transfer irreversibility becomes increasingly intense and influential.

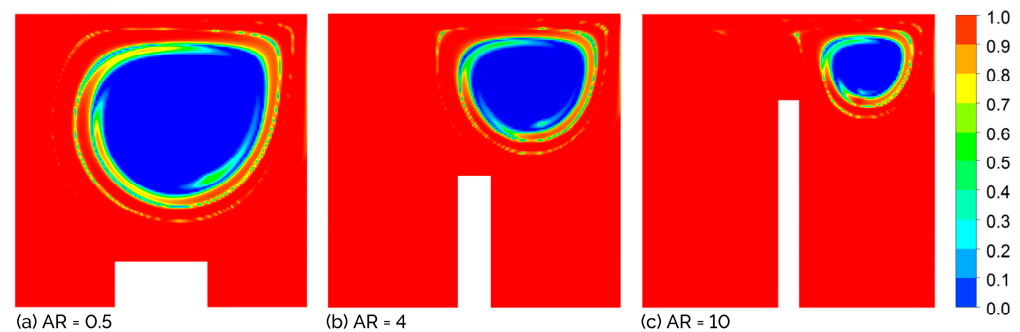


Figure 11. Contour plots of Bejan number for $Ra = 10^5$, $Re = 1000$, and fin area fraction of 0.05 for three fin aspect ratios. (a) $AR = 0.5$, (b) $AR = 4$, and (c) $AR = 10$.

5. Conclusions

A parametric numerical investigation has been performed to study the mixed convection of CuO-water nanofluid in a square lid-driven cavity with a moving top wall and an intruded rectangular fin to provide insight into enhanced thermal properties and heat transfer through geometry optimization. The present study highlights the impact of fin geometry in convective heat transfer from the fin surface to the surrounding nanofluid. The flow resistance caused by the higher fin aspect ratio is significant. The increase in the fin surface area with fin aspect ratio may not provide a higher heat transfer from the fin surface to the surrounding nanofluid, which indicates the importance of the constructal design method for the optimization of mixed convective flow problems. The present results show that Rayleigh numbers have limited effects, while aspect ratios close to a value of 0.5 to 2 seem to behave more efficiently with the nanofluid. For the mixed convection dominant flow, the buoyancy force influences the heat transfer greatly at higher Rayleigh numbers. On top of that, the dominance of each entropy generation mode depends on the fin geometry and for higher aspect ratios the entropy generation is mostly caused due to inertial forces between the particles. Undoubtedly, it is of great importance to know the cause of entropy generation, a form of energy that is no longer useful, and, therefore, will be able to minimize it to allow the system to be much more efficient, and less energy consuming. Present results further indicate that the concentration of CuO-nanoparticles can enhance both conduction and convection heat transfer to that of the base fluid and lower entropy generation, which will be useful for electronic devices, energy conversion/storage, and related applications, particularly in improving heat removal for electronic devices, in increasing heat transfer performance in solar collectors for hot water supply and enhancing energy efficiency and the cooling of nuclear rods in a nuclear power plant by improving the functionality of the existing system.

Author Contributions: Conceptualization, W.Z. and P.K.D.; methodology, P.M., W.Z. and M.S.R.; validation, P.M. and W.Z.; formal analysis, P.M., W.Z., M.S.R. and P.K.D.; investigation, P.M., W.Z. and M.S.R.; data curation, P.M. and W.Z.; writing—original draft preparation, P.M. and W.Z.; writing—review and editing, P.M. and P.K.D.; supervision, P.K.D.; project administration, P.K.D. All authors have read and agreed to the published version of the manuscript.

Funding: This research received no external funding.

Data Availability Statement: Not applicable.

Conflicts of Interest: The authors declare no conflict of interest.

References

1. Cong, R.; Ozaki, Y.; Machado, B.S.; Das, P.K. Constructal design of a rectangular fin in a mixed convective confined environment. *Inventions* **2018**, *3*, 27. [\[CrossRef\]](#)
2. Shi, X.; Khodadadi, J.M. Laminar fluid flow and heat transfer in a lid-driven cavity due to a thin fin. *J. Heat Transf.* **2002**, *124*, 1056–1063. [\[CrossRef\]](#)
3. Razera, A.L.; da Fonseca, R.J.C.; Isoldi, L.A.; dos Santos, E.D.; Rocha, L.A.O.; Biserni, C. Constructal design of a semi-elliptical fin inserted in a lid-driven square cavity with mixed convection. *Int. J. Heat Mass Transf.* **2018**, *126*, 81–94. [\[CrossRef\]](#)
4. Ting, K.; Mozumder, A.K.; Das, P.K. Effect of surface roughness on heat transfer and entropy generation of mixed convection in nanofluid. *Phys. Fluids* **2019**, *31*, 093602. [\[CrossRef\]](#)
5. Yang, O.A.W.-J. Mixed convection in cavities with a locally heated lower wall and moving sidewalls. *Numer. Heat Transf. Part A Appl.* **2000**, *37*, 695–710. [\[CrossRef\]](#)
6. Ilis, G.G.; Mobedi, M.; Sunden, B. Effect of aspect ratio on entropy generation in a rectangular cavity with differentially heated vertical walls. *Int. Commun. Heat Mass Transf.* **2008**, *35*, 696–703. [\[CrossRef\]](#)
7. Oztop, H.F.; Abu-Nada, E. Numerical study of natural convection in partially heated rectangular enclosures filled with nanofluids. *Int. J. Heat Fluid Flow* **2008**, *29*, 1326–1336. [\[CrossRef\]](#)
8. Basak, T.; Roy, S.; Sharma, P.K.; Pop, I. Analysis of mixed convection flows within a square cavity with uniform and non-uniform heating of bottom wall. *Int. J. Therm. Sci.* **2009**, *48*, 891–912. [\[CrossRef\]](#)
9. Mahmud, S.; Das, P.K.; Hyder, N.; Islam, A.K.M.S. Free convection in an enclosure with vertical wavy walls. *Int. J. Therm. Sci.* **2002**, *41*, 440–446. [\[CrossRef\]](#)
10. Nayak, R.K.; Bhattacharyya, S.; Pop, I. Numerical study on mixed convection and entropy generation of Cu–water nanofluid in a differentially heated skewed enclosure. *Int. J. Heat Mass Transf.* **2015**, *85*, 620–634. [\[CrossRef\]](#)
11. Das, P.K.; Mahmud, S. Effect of eccentricity and radius ratio on fluid flow and heat transfer inside an eccentric semicircular enclosure. *J. Therm. Sci.* **2000**, *9*, 135–140. [\[CrossRef\]](#)
12. Mahmud, S.; Das, P.K.; Hyder, N. Laminar natural convection around an isothermal square cylinder at different orientations. *Int. Commun. Heat Mass Transf.* **2002**, *29*, 993–1003. [\[CrossRef\]](#)
13. Tasnim, S.H.; Mahmud, S.; Das, P.K. Effect of aspect ratio and eccentricity on heat transfer from a cylinder in a cavity. *Int. J. Numer. Methods Heat Fluid Flow* **2002**, *12*, 855–869. [\[CrossRef\]](#)
14. Das, P.K.; Mahmud, S. Numerical investigation of natural convection inside a wavy enclosure. *Int. J. Therm. Sci.* **2003**, *42*, 397–406. [\[CrossRef\]](#)
15. Das, P.K.; Mahmud, S.; Tasnim, S.H.; Islam, A.K.M.S. Effect of surface waviness and aspect ratio on heat transfer inside a wavy enclosure. *Int. J. Numer. Methods Heat Fluid Flow* **2003**, *13*, 1097–1122. [\[CrossRef\]](#)
16. Buongiorno, J. Convective transport in nanofluids. *J. Heat Transf.* **2006**, *128*, 240–250. [\[CrossRef\]](#)
17. Ji, Y.; Zhang, H.-C.; Yang, X.; Shi, L. Entropy generation analysis and performance evaluation of turbulent forced convective heat transfer to nanofluids. *Entropy* **2017**, *19*, 108. [\[CrossRef\]](#)
18. Khanafer, K.; Vafai, K.; Lightstone, M. Buoyancy-driven heat transfer enhancement in a two-dimensional enclosure utilizing nanofluids. *Int. J. Heat Mass Transf.* **2003**, *46*, 3639–3653. [\[CrossRef\]](#)
19. Lee, S.; Choi, S.U.-S.; Li, S.; Eastman, J.A. Measuring thermal conductivity of fluids containing oxide nanoparticles. *J. Heat Transf.* **1999**, *121*, 280–289. [\[CrossRef\]](#)
20. Choi, S.U.S. *Enhancing Thermal Conductivity of Fluids with Nanoparticles*; ASME International Mechanical Engineering Congress and Exposition: San Francisco, CA, USA, 1995; pp. 99–105.
21. Wong, K.V.; De Leon, O. Applications of nanofluids: Current and future. *Adv. Mech. Eng.* **2010**, *2*, 519659. [\[CrossRef\]](#)
22. Tiwari, R.K.; Das, M.K. Heat transfer augmentation in a two-sided lid-driven differentially heated square cavity utilizing nanofluids. *Int. J. Heat Mass Transf.* **2007**, *50*, 2002–2018. [\[CrossRef\]](#)
23. Talebi, F.; Mahmoudi, A.H.; Shahi, M. Numerical study of mixed convection flows in a square lid-driven cavity utilizing nanofluid. *Int. Commun. Heat Mass Transf.* **2010**, *37*, 79–90. [\[CrossRef\]](#)
24. Mansour, M.A.; Mohamed, R.A.; Abd-Elaziz, M.M.; Ahmed, S.E. Numerical simulation of mixed convection flows in a square lid-driven cavity partially heated from below using nanofluid. *Int. Commun. Heat Mass Transf.* **2010**, *37*, 1504–1512. [\[CrossRef\]](#)
25. Atashafrooz, M. The effects of buoyancy force on mixed convection heat transfer of MHD nanofluid flow and entropy generation in an inclined duct with separation considering Brownian motion effects. *J. Therm. Anal. Calorim.* **2019**, *138*, 3109–3126. [\[CrossRef\]](#)
26. Atashafrooz, M.; Sajjadi, H.; Amiri Delouei, A.; Yang, T.-F.; Yan, W.-M. Three-dimensional analysis of entropy generation for forced convection over an inclined step with presence of solid nanoparticles and magnetic force. *Numer. Heat Transf. Part A Appl.* **2021**, *80*, 318–335. [\[CrossRef\]](#)
27. Hong, T.; Yang, H.; Choi, C.J. Study of the enhanced thermal conductivity of Fe nanofluids. *J. Appl. Phys.* **1997**, *205*, 064311. [\[CrossRef\]](#)
28. Bejan, A. *Convection Heat Transfer*, 4th ed.; John Wiley & Sons: Hoboken, NJ, USA, 2013.
29. Bejan, A. From heat transfer principles to shape and structure in nature: Constructal theory. *J. Heat Transf.* **2000**, *122*, 430–449. [\[CrossRef\]](#)
30. Bejan, A.; Almgöbel, M. Constructal T-shaped fins. *Int. J. Heat Mass Transf.* **2000**, *43*, 2101–2115. [\[CrossRef\]](#)
31. Bejan, A.; Lorente, S. Design with constructal theory. *Int. J. Eng. Educ.* **2006**, *22*, 140–147.

32. Lorenzini, G.; Moretti, S. A CFD application to optimize t-shaped fins: Comparisons to the constructal theory's results. *J. Electron. Packag.* **2007**, *129*, 324–327. [[CrossRef](#)]
33. Lorenzini, G.; Medici, M.; Rocha, L.A.O. Convective analysis of constructal T-shaped fins. *J. Eng. Thermophys.* **2014**, *23*, 98–104. [[CrossRef](#)]
34. Lorenzini, G.; Machado, B.S.; Isoldi, L.A.; dos Santos, E.D.; Rocha, L.A.O. Constructal design of rectangular fin intruded into mixed convective lid-driven cavity flows. *J. Heat Transf.* **2016**, *138*, 102501. [[CrossRef](#)]
35. Cong, R.; Zhou, X.; Machado, B.D.S.; Das, P.K. Mixed convection flow of nanofluid in a square enclosure with an intruded rectangular fin. *AIP Conf. Proc.* **2016**, *1754*, 050017.
36. Cho, C.-C. Heat transfer and entropy generation of natural convection in nanofluid-filled square cavity with partially-heated wavy surface. *Int. J. Heat Mass Transf.* **2014**, *77*, 818–827. [[CrossRef](#)]
37. Oliveski, R.D.C.; Macagnan, M.H.; Copetti, J.B. Entropy generation and natural convection in rectangular cavities. *Appl. Therm. Eng.* **2009**, *29*, 1417–1425. [[CrossRef](#)]
38. Das, P.K.; Li, X.; Liu, Z.S. Effective transport coefficients in PEM fuel cell catalyst and gas diffusion layers: Beyond Bruggeman approximation. *Appl. Energy* **2010**, *87*, 2785–2796. [[CrossRef](#)]
39. Zhao, W.; Mozumder, A.K.; Das, P.K. Mixed convection of CuO-water nanofluid in a square enclosure with an intruded rectangular fin. *AIP Conf. Proc.* **2018**, *1980*, 050004.
40. Izadi, M.; Shahmardan, M.M.; Behzadmehr, A. Richardson number ratio effect on laminar mixed convection of a nanofluid flow in an annulus. *Int. J. Comput. Methods Eng. Sci. Mech.* **2013**, *14*, 304–316. [[CrossRef](#)]
41. Bejan, A.; Kestin, J. Entropy generation through heat and fluid flow. *J. Appl. Mech.* **1983**, *50*, 475. [[CrossRef](#)]
42. Nallasamy, M.; Prasad, K.K. On cavity flow at high Reynolds numbers. *J. Fluid Mech.* **1977**, *79*, 391–414. [[CrossRef](#)]
43. Dixit, H.N.; Babu, V. Simulation of high Rayleigh number natural convection in a square cavity using the lattice Boltzmann method. *Int. J. Heat Mass Transf.* **2006**, *49*, 727–739. [[CrossRef](#)]

Disclaimer/Publisher's Note: The statements, opinions and data contained in all publications are solely those of the individual author(s) and contributor(s) and not of MDPI and/or the editor(s). MDPI and/or the editor(s) disclaim responsibility for any injury to people or property resulting from any ideas, methods, instructions or products referred to in the content.